



On the modeling of external mass transfer phenomena in Pd-based membrane separations

W.J.R. Ververs^a, M. Ongis^{a,b}, A. Arratibel^c, L. Di Felice^a, F. Gallucci^{a,d,*}

^a Inorganic Membranes and Membrane Reactors, Sustainable Process Engineering, Department of Chemical Engineering and Chemistry, Eindhoven University of Technology, P.O. Box 513, 5600 MB, Eindhoven, the Netherlands

^b Group of Energy Conversion Systems, Department of Energy, Politecnico di Milano, via Lambruschini 4a, 20156, Milan, Italy

^c TECNALIA, Basque Research and Technology Alliance (BRTA), Mikeletegi Pasealekua 2, 20009, Donostia-San Sebastian, Spain

^d Eindhoven Institute for Renewable Energy Systems (EIRES), Eindhoven University of Technology, P.O. Box 513, 5600 MB, Eindhoven, the Netherlands

ARTICLE INFO

Handling editor: Mehran Rezaei

Keywords:

Hydrogen selective membranes
Concentration polarization
Mass transfer coefficient
Sherwood correlations

ABSTRACT

In this work, external mass transfer phenomena around hydrogen selective Pd-based membranes were analyzed experimentally and mathematically modelled. A supported Pd-Ag membrane was tested in pure hydrogen and in hydrogen/nitrogen mixtures using three different membrane lengths. Pressure, temperature, gas flow rate and feed composition were varied to obtain an elaborate dataset that could be used for analysis and modelling. Strong influences of concentration polarization and hydrogen depletion were observed. Various empirical correlations describing gas phase mass transfer around a tubular membrane from literature were tested, but none of them yielded a sufficiently accurate prediction of concentration polarization observed in the experiments. Therefore, a new Sherwood correlation was fitted using the dataset. The obtained correlation ($Sh = 1.846 \cdot Gz^{0.60}$) showed significantly improved predictive behavior for the system used in this work and represents a potentially powerful tool for the modelling of membrane separators for pure hydrogen production.

1. Introduction

The recently abundant signs of climate changes due to global warming, like melting glaciers and rising sea levels, have reminded us that we need to improve and redesign our energy supply industry. These climate changes are directly due to anthropogenic greenhouse gases emissions. As a consequence, it is clear that fossil-based fuels cannot be used as energy source in the foreseeable future, since this would have detrimental consequences for life on earth [1]. Therefore, new energy carriers and energy sources are highly needed. Currently, hydrogen is considered as one of the most advanced and highest potential candidates of (partially) fulfilling the gap that fossil-based energy industry will leave behind [2]. Many different processes for clean and energy-efficient hydrogen production are being developed. Not all these processes have a pure hydrogen product stream directly from the reactor. Therefore, additional separation steps are required to ensure a hydrogen purity that matches the requirements of the unit that will convert the hydrogen back to the energy form that is needed (such as fuel cells). The energy consumption of these separation steps directly reduces the energy

efficiency of the energy carrier system. Membrane separation can be used to reduce the energy demand of the hydrogen purification steps [3].

Specifically, Pd-based membranes have a high permeance and perm-selectivity, meaning that they can separate a significant amount of hydrogen at a purity that could match the high purity requirements that hydrogen fuel cells need [4]. These membranes can be used both in a separator unit for gas mixtures such as methane/hydrogen mixtures (interesting for hydrogen storage in natural gas grids) as well as in an integrated membrane reactor for production and recovery of hydrogen from different fuels/hydrogen carriers (methane, ethanol, methanol ammonia) [5–15].

The currently available Pd-based membranes are close to ready for commercial implementation and production lines for Pd-based membranes have been developed [16]. Membranes can be produced with hydrogen permeance of $5 \cdot 10^{-6} \text{ mol s}^{-1} \text{ m}^{-2} \text{ Pa}^{-1}$ and an ideal H_2/N_2 perm-selectivity higher than 25,000 [17]. While the development of the membranes is going fast, a demand for practical and accurate modelling of membrane systems is created. The membrane permeance itself is

* Corresponding author. Inorganic Membranes and Membrane Reactors, Sustainable Process Engineering, Department of Chemical Engineering and Chemistry, Eindhoven University of Technology, P.O. Box 513, 5600 MB, Eindhoven, the Netherlands.

E-mail address: f.gallucci@tue.nl (F. Gallucci).

<https://doi.org/10.1016/j.ijhydene.2024.04.337>

Received 20 February 2024; Received in revised form 18 April 2024; Accepted 28 April 2024

Available online 25 May 2024

0360-3199/© 2024 The Authors. Published by Elsevier Ltd on behalf of Hydrogen Energy Publications LLC. This is an open access article under the CC BY license (<http://creativecommons.org/licenses/by/4.0/>).

relatively simple to model using Richardson's equation, which calculates the hydrogen flux based on the hydrogen partial pressures at the outer and inner surface of the membrane. However, due to the high permeance of the membranes, external mass transfer (limitation) becomes a highly important factor impacting the hydrogen flux. This influence of external mass transfer on the overall behavior of a membrane system is often referred to as *concentration polarization*. The impact of external mass transfer limitations may result in a required membrane area significantly higher compared to the one evaluated without considering the mass transfer limitations [18].

Many authors already reported the importance of this phenomenon, and several different methods have been suggested to analyze or predict it [19–23]. However, external mass transfer is known to be a complex phenomenon to predict using a model. CFD models are often used to generate better understanding of different parameters of membrane integrated systems, but validation with experimental data from Pd-based membranes is difficult and simulations are time consuming. An approach with a more simplified model can be used to predict the behavior of a membrane integrated process. Many different research developed models predicting the separation performance of Pd-based membranes in an empty vessel using an empirical expression [19,20,23–28]. The approach that these works is to consider a mass transfer film layer around the membrane where the external transport resistance takes place. Transport in this specific layer is then described using a mass transfer coefficient which is calculated from an empirical Sherwood correlation. The differences among these works lie in the formulations of the Sherwood correlation. Caravella et al. used a correlation based on the analytical derivation of a simplified mass transfer problem [19,25]. Catalano et al. fitted a correlation based on an experimental dataset [20,24]. And Brencio et al., Nordio et al. and Boon et al. used a constant Sherwood number for all conditions [21,27,28]. In general, there is a clear lack of unified approach as well as understanding of the phenomena and how to implement those in the models. The assumed Sherwood numbers are sometimes not applicable to the case studied and large errors in terms of membrane area required would be generated by improperly using those equations.

The objective of this work is to experimentally analyze external mass transfer behavior of a highly permeable supported Pd-Ag membrane in an empty vessel. The dataset obtained from the experimental tests will be used to evaluate the different external mass transfer correlations used in literature and to give clarity on the applicability of those equations. Finally, a new mass transfer correlation will be fitted and compared to other correlations from literature. Additionally, the obtained experimental dataset will be made available in the supplementary data and stored open access at Zenodo, such that it can be used by other investigators [29].

2. Materials and methods

2.1. Membranes

The membrane used in this work is a supported Pd-Ag membrane, prepared via simultaneous electroless plating according to the procedure described by Arratibel et al. [17]. The support was a finger-like asymmetric α -Al₂O₃ support (pore size of 0.1 μ m at the outer surface and 3 μ m at the inner side), provided by Rauschert Kloster Veilsdorf. The membrane has a length of 467 mm and an OD/ID ratio of 14/7 mm, where OD and ID are the outer and inner diameter of the tubular membrane. The thickness of the Pd-Ag layer was determined by performing a Scanning Electron Microscopy (SEM) on the cross-section.

2.2. Membrane tests

The membrane tests were performed in an experimental setup designed for the characterization of Pd-based membranes. The experimental setup contains a gas feed section with mass flow controllers

provided by Bronkhorst. The feed gas was fed through a CAST-X 500 gas heater provided by KURVAL. The gas was then led through a spiral into the membrane module, both heated by a Carbolite-Gero TF3 three-zone tubular oven provided by VERDER scientific. The membrane module consisted of a stainless-steel vessel with an internal diameter of 78 mm. The retentate outlet of the membrane module was cooled in a heat-exchanger and then sent to a back-pressure controller provided by Bronkhorst. The permeate outlet was sent to a thermal mass flow meter also provided by Bronkhorst. Temperature was monitored using a multi-point thermocouple monitoring the temperature at 8 different points in the module. Layout of the testing setup is reported in Fig. 1.

The permeation behavior of the membrane was tested at three different lengths – 467 mm, 300 mm, and 150 mm –, to investigate the effect of the membrane length and to increase the amount of data that can be used for modelling. This was done by testing the membrane at full length, followed by cutting off the sealed edges and re-sealing – after which the membrane could be tested again. Every time the membrane was tested, it was activated in air for 2 min at 400 °C and kept in pure hydrogen atmosphere until a stable permeance was observed. The membrane tests consisted of pure hydrogen permeation measurements varying temperature and pressure to determine the Richardson's parameters and H₂/N₂ mixture tests to investigate external mass transfer behavior. For each length, both pure hydrogen and mixture tests were performed at 450 °C, then at 400 °C and lastly at 350 °C. The membrane test procedure is visualized in Fig. 2.

3. Modelling

To model the hydrogen permeation through a dense Pd-based membrane, every mass transfer step contributing significantly to the observed flux must be included. For a Pd-based membrane in pure hydrogen, the transport resistances are induced by the Pd-based layer and the support. Hydrogen transport through the Pd-based layer follows the solution-diffusion mechanism, since a H₂ molecule first undergoes dissociative adsorption, then the atoms diffuse through the Pd-based layer and finally undergoes associative desorption. Richardson's equation is required to model the transport through the Pd-based layer [30].

$$N_{H_2} = Pe_0 \exp\left(-\frac{E_a}{RT}\right) \left[(p_{H_2, \text{memb}})^n - (p_{H_2, \text{perm}})^n \right] \quad (1)$$

N_{H_2} is the permeating hydrogen flux, Pe_0 is the pre-exponential factor of permeance, E_a is the apparent activation energy, n is the pressure exponent and $p_{H_2, \text{memb}}$ and $p_{H_2, \text{perm}}$ are the hydrogen partial pressures next to the retentate and permeate side surfaces of the membrane. Additionally, also the resistance of the porous support can be lumped into the parameters of Richardson's equation [31].

The purpose of Pd-based membranes is of course to remove hydrogen from a gas mixture, so the hydrogen fraction and total gas flow rate will decrease along the length of the membrane. Reduction in hydrogen molar fraction is typically denoted as depletion, and it can have a significant impact on the overall membrane flux, since it is directly related to hydrogen partial pressure (the relation $p_{H_2} = p \cdot x_{H_2}$ is assumed to be valid in the applied operating conditions). Therefore, at least a 1D discretization of the membrane area is required, such that the changing composition and gas velocity reduction along the module can be accounted for. The membrane was discretized only in the axial direction since the system is symmetrical in the angular direction, as visualized in Fig. 3. The radial direction will be accounted for in the external mass transfer term.

After discretizing the gas-phase around the membrane (i.e. retentate), a system with unit-cells in the shape of annular discs is obtained. The gas flow follows the upward vertical direction (z), and the permeation flux follows the radial direction (y). A mass balance for hydrogen and other components (i) can then be formulated for each unit cell.

$$0 = F_{H_2, z} - F_{H_2, z+\Delta z} - N_{H_2, z} \cdot dA \quad (2)$$

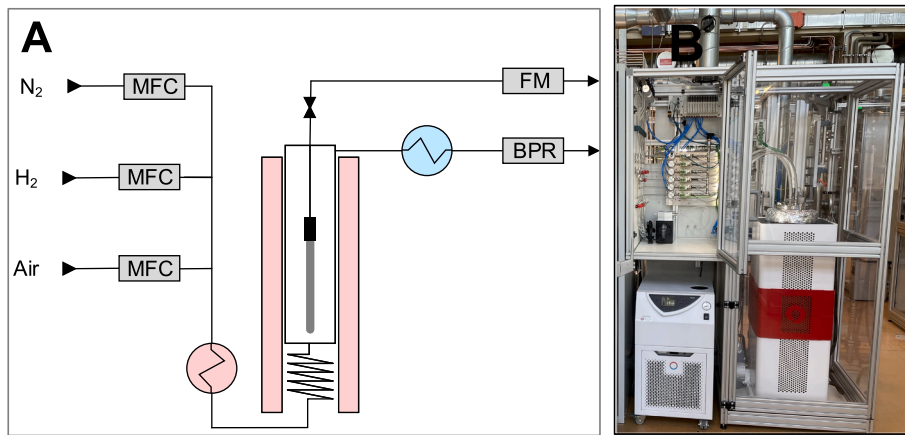


Fig. 1. Process flow diagram (A) and picture (B) of the experimental test setup used in this work. MFC = mass flow meter; FM = flow meter; BPR = back pressure regulator.

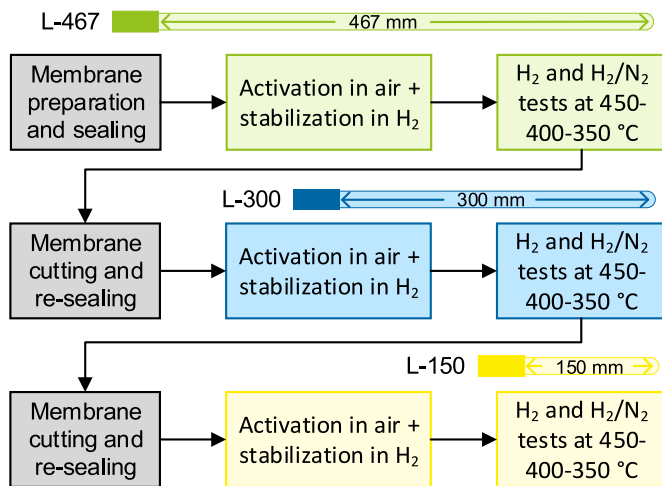


Fig. 2. Visualization of the membrane test procedure including cutting and re-sealing steps.

$$0 = F_{N_2,z} - F_{N_2,z+\Delta z} \quad (3)$$

$F_{N_2,z}$ is the molar flow of nitrogen at position z and $F_{H_2,z}$ is the molar permeation flux of hydrogen at position z and A is the membrane surface area. The molar permeation flux of hydrogen is described by the

permeation model. Since Pd-based membranes are highly perm-selective, only the permeation flux of hydrogen is considered, while for the other components (nitrogen) it is assumed to be equal to zero.

The permeation flux is calculated using Richardson’s equation (Equation (1)), which relates the hydrogen flux to the pressures at the inner and outer surfaces of the membrane. Due to external mass transfer resistance, a difference in hydrogen partial pressure between the bulk and the outer membrane surface is created. To calculate the partial pressure of hydrogen at the membrane surface, an external mass transfer model should be used. The most common approach of modelling external mass transfer is by considering it as a film layer at the membrane surface, where the rate of mass transport is described via a mass transfer coefficient. Stagnant film model formulation for a bicomponent gas mixture in cylindrical geometry has already been formulated by Nooijer et al., describing hydrogen permeation in Pd-based membranes in a fluidized bed membrane reactor for methane reforming [32]. The equation describing the hydrogen flux through a boundary layer of thickness δ at the surface of a cylindrical membrane of radius r_{memb} is reported in Equation (4). The first term of the equation can be grouped under an overall mass transfer coefficient k_g . The approach using the film model has some flaws that suggest that it is not completely fundamentally correct according to a recently published work of Song et al. [33]. However, in practice it is the most applied way of modelling concentration polarization for membranes, meaning that it is quite effective at modeling the mass transfer rate.

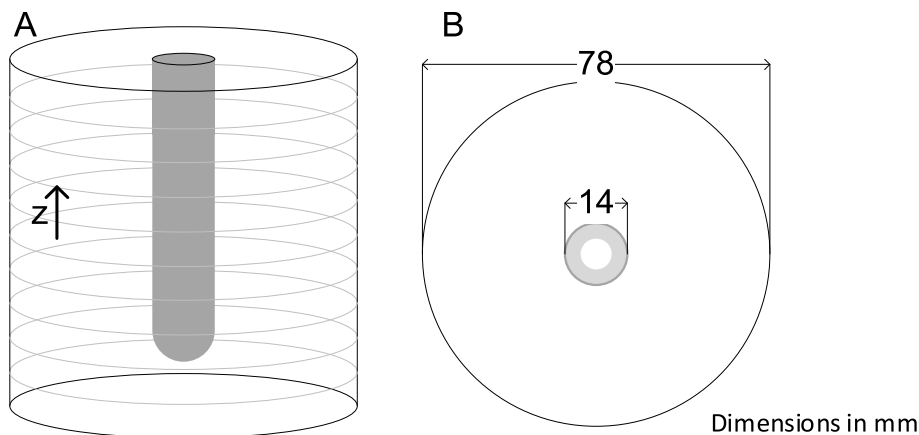


Fig. 3. Schematic drawings of the membrane inside the vessel. A) discretization in the axial direction; B) cross-section projection with dimensions of the membrane and the vessel.

$$N_{H_2}(r_{\text{memb}}) = \frac{D_{H_2-N_2}}{r_{\text{memb}} \ln\left(1 + \frac{\delta}{r_{\text{memb}}}\right)} c_{\text{tot}} \ln\left(\frac{1 - x_{H_2,\text{memb}}}{1 - x_{H_2,\text{bulk}}}\right) \quad (4)$$

$$= k_g c_{\text{tot}} \ln\left(\frac{1 - x_{H_2,\text{memb}}}{1 - x_{H_2,\text{bulk}}}\right)$$

If the mass transfer coefficient is known, the equations above can be solved numerically to obtain the overall hydrogen flux. The required mass transfer coefficient however is strongly dependent on the geometry and stream properties around the membrane, and thus is very case specific. The most common interpretation of the stagnant film model has been mathematically justified by Zydney and assumes that the mass transfer coefficient k_g can be interpreted as the convective coefficient using a pseudo-concentration [34]. The same approach has been used by Rohlf's et al., and allows to justify the determination of the mass transfer coefficient starting from the knowledge of the Sherwood number, which is defined as the ratio of the rates of convective and diffusive mass transport [35].

$$Sh = \frac{k_g d_h}{D_{H_2-N_2}} \quad (5)$$

The final step is to calculate the Sherwood number, for this, an empirical correlation is typically used. In literature a wide range of different correlations is available for a huge variety of different systems. Part of his work will focus on Sherwood correlations that can be used to determine the mass transfer coefficient in a system with a Pd-based membrane in an empty vessel.

4. Results and correlations fitting

4.1. Experimental results of pure gas tests

The membrane was tested at each length for its permeation behavior in pure hydrogen, while the pressure was varied between 1.5 and 5 bar (a) at 450-400-350 °C. In Table 1, the permeance Pe and ideal H_2/N_2 perm-selectivity, S_{H_2/N_2} of the different membrane lengths are compared to each other and to works of similar membranes in literature. Permeance is defined as the hydrogen *trans*-membrane flux divided by the difference in hydrogen partial pressure. The ideal H_2/N_2 perm-selectivity is defined as the ratio of the membrane fluxes in both pure hydrogen and pure nitrogen at the same pressure. The obtained membrane parameters are in line with results of other works found in literature. The perm-selectivity decreased significantly during the testing period and during cutting and re-sealing of the membrane. Since the selectivity remains still above 1,000, it can be reasonably assumed that the permeation behavior is unaffected by non-selective permeation as already reported in literature. When the hydrogen permeances of the different membrane lengths are compared, slight differences are observed. This could be caused by changing surface properties as a result of (re-)activation, temperature cycles or ageing of the membrane. Additionally, local differences in surface properties and selective layer

thickness could also lead to different permeation behavior, these local differences would become noticeable in the parameters when removing part of the membrane. However, it is important to stress that these differences are very small, and the membranes can therefore be considered as near identical in terms of hydrogen permeation properties.

The data obtained from the pure hydrogen permeation tests were used to fit the parameters of Richardson's equation for each membrane length. The fitted Richardson parameters are shown in Table 1. In Fig. 4, the pure hydrogen permeation data is visualized together with the predictions of Richardson's equation using the fitted values. The experimental datapoints closely match the model's predictions, meaning that the parameters were properly fitted.

The values of the Richardson parameters reported in Table 1 are in line with values reported for other supported Pd-Ag membranes. The observed value of the pressure exponent n , is higher than 0.5, indicating that internal diffusion is not the only step affecting the permeation rate [25,31,38]. In thin Pd-based membranes, the diffusion step is sufficiently fast, such that the effects of the adsorption and/or desorption rates become visible in the overall permeation rate. Besides that, also external transport steps like the mass transfer resistance in the porous support can also become significant for highly permeable membranes. These "non-idealities" with respect to the assumptions leading to a pressure exponent of 0.5 (Sieverts' law) can lead to the increased value (maximum up to 1) of the pressure exponent [25]. The differences in terms of activation energy are generally difficult to explain since various effects tend to alter this value. The differences observed in Table 1 are considered quite small and are therefore, just like the overall permeance, attributed to local differences on the membranes and to repeated activation procedures.

4.2. Experimental results of hydrogen/nitrogen mixture tests

Extensive H_2/N_2 mixture tests were performed at 450-400-350 °C. The feed pressure, flow rate and composition were varied to study the mass transfer behavior around the Pd-based membrane. Details of the conditions applied in these mixture tests can be found in Supplementary data 1, as well as the complete dataset of experimental results obtained in this work. The dataset consists of 423 datapoints in total, the test conditions were equal for each membrane at each applied temperature. The datasets are made available in the supplementary files and at Zenodo [29].

Fig. 5 shows a small sample of the dataset with varied feed flow rate for each membrane length. The x-axis shows the A/F ratio which represents the ratio between membrane area and feed total flow rate. This parameter can be useful to visualize permeation data of multiple membranes with different lengths (or areas), since it shows the amount of hydrogen fed relative to the membrane area available for hydrogen removal. The y-axis shows the recovery factor of hydrogen RF, which is generally defined with the following equation, as the ratio between hydrogen separated and hydrogen fed.

Table 1

Comparison of properties and fitted Richardson parameters for each of the three membrane lengths of 467 mm (L-467), 300 mm (L-300) and 150 mm (L-150) used in this work.

	This work			Other works			
	L-467	L-300	L-150	[36]	[37]	[24]	[32]
t (μm)	4.3			1.3	2.4	2.5	5.2
L (mm)	467	300	150	58	30	90	143.5
Pe* (mol s ⁻¹ m ⁻² bar ⁻¹)	0.184	0.174	0.192	0.9	0.75	0.473	0.21**
S _{H₂/N₂} *	53,919	10,589	1,406	3,300	2,140	10,000	4,576**
Pe ₀ (× 10 ⁻³ mol s ⁻¹ m ⁻² Pa ⁻ⁿ)	2.187	2.669	2.968				
E _a (kJ/mol)	9.684	9.262	10.451	7.44	4.4	7.8	9.23
n	0.594	0.581	0.584	0.64	0.71	0.5	0.5

* 2 bar(a) and 400 °C.

** 384 °C instead of 400 °C.

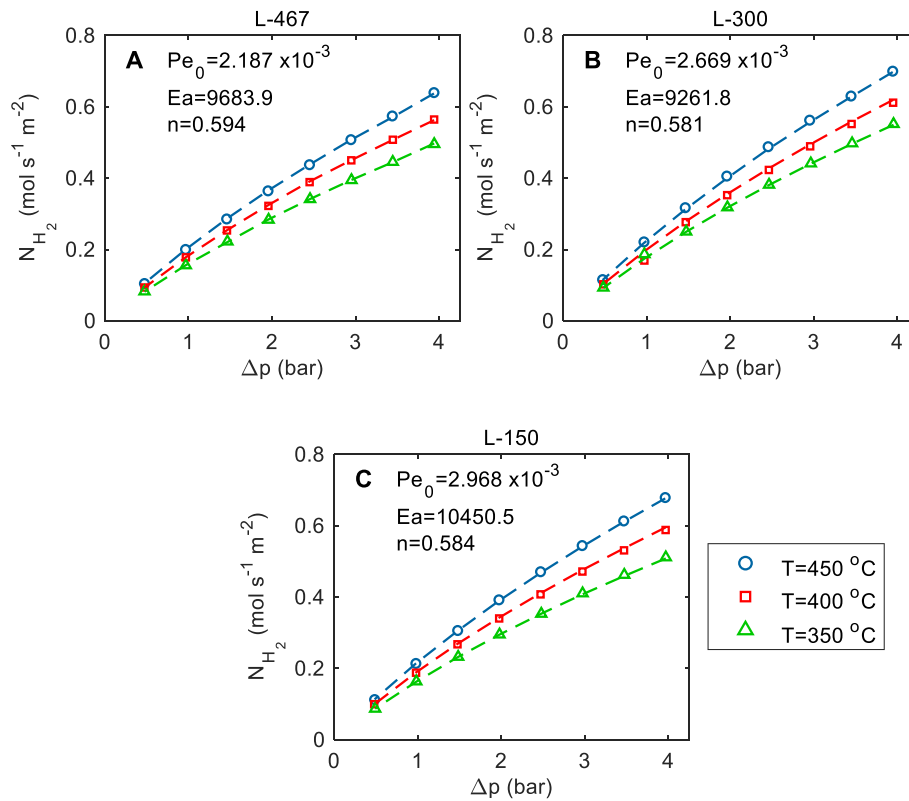


Fig. 4. Fitted and experimental hydrogen flux versus pressure drop at different temperature for the three different membrane lengths A) 467 mm (L-467), B) 300 mm (L-300), and C) 150 mm (L-150).

$$F_{H_2, \text{separated}} = RF \cdot F_{H_2, \text{feed}} \Rightarrow RF = \frac{F_{H_2, \text{separated}}}{F_{H_2, \text{feed}}} \quad (6)$$

In Fig. 5, also the results of a model neglecting any external mass transfer resistance are shown as solid lines for comparison.

The data in Fig. 5 shows that the recovery factor increases as the A/F ratio increases for all cases. A higher A/F ratio induces a higher RF since more hydrogen is separated when there is a larger membrane area. However, the slope of the curves progressively decreases also in the ideal model, indicating that hydrogen depletion (i.e. reduction of hydrogen concentration due to selective permeation) is an important phenomenon to be considered in any model. The lines of the ideal model reach an asymptote somewhat below 1, since hydrogen can be separated only until its partial pressure is higher than the equivalent partial pressure in the permeate side. The gaps between the lines of the model without concentration polarization and the experimental datapoints demonstrate the presence of concentration polarization, of which impact was already highlighted by various authors [19–23,27]. For all the parameters investigated (temperature, feed pressure, hydrogen inlet molar fraction) the model without CP highly overestimates the hydrogen separation, showing that it is necessary to properly include their description in the model.

Besides the appearance of concentration polarization and hydrogen depletion effects, it can also be seen that the mass transfer behavior is quite similar for each membrane length experimentally studied, since data for the 150 mm, 300 mm and 467 mm membranes seem to lie on a single line.

4.3. External mass transfer modelling from literature

The analysis of the results obtained during the binary mixture experiments highlighted the occurrence of two important effects taking place in a Pd-based membrane system, namely, hydrogen depletion and concentration polarization. The effect of depletion is accounted for in

the model by discretizing the membrane surface in the axial direction, as was described in the description of the model. To account for concentration polarization, a relevant empirical Sherwood correlation must be used to complete the film layer model described before.

The Sherwood number can be calculated from a correlation relevant for the geometry of the system and the conditions of the application. Sherwood correlations for regular systems (e.g. flow through a pipe, around a sphere, etc.) are widely available, however to the best of the author's knowledge a versatile correlation for forced parallel flow in a pipe around highly permeable cylindrical membranes has not been investigated yet. Other works in literature with similar configurations use a variety of different correlations, some adopted from systems with similarities, and some fitted using data experimental data of membrane separators. Eight different examples of the correlations used in literature can be found in Table 2.

The correlations shown in Table 2 show clear differences, both in terms of values of the empirical coefficients and in terms of the general form of the equation. There are expressions for average Sherwood numbers that apply for the entire length of the membrane indicated with \bar{Sh}_L [20,21,24,27,28]; other authors refer to local Sherwood numbers which are depending on the axial coordinate indicated with Sh_z [19,25,40]. This is an important difference, since on one side it is important to account for conditions changing along the membrane. However, on the other side, simplicity is desired for an empirical correlation, because overfitting might make the modelling work case-specific or applicable only in a very limited range of conditions. Another difference among the correlations is the calculation of the hydraulic diameter, since either the general definition of the hydraulic diameter, or the membrane length, have been found to be used in the reported literature. To create a systematic way of calculating the hydraulic diameter, a definition was given in Ref. [40].

$$d_h = \frac{4A_c}{P} \quad (7)$$

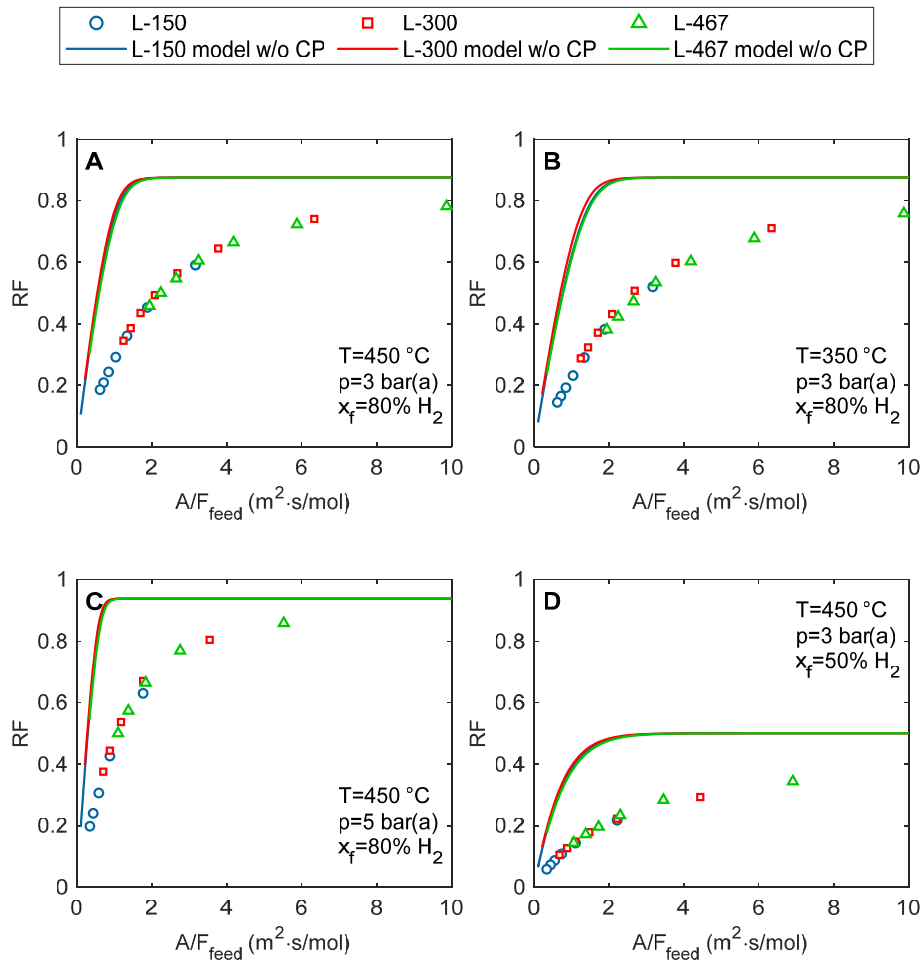


Fig. 5. Results of experiments and ideal model (no CP) of H₂/N₂ permeation tests. Datapoints are expressed in recovery factor RF and area-to-feed flow ratio A/F_{feed}. A) shows results at 450 °C, 3 bar(a) and 80% hydrogen (base case), B) at lower temperature, C) at higher pressure and D) at lower hydrogen feed fraction.

Table 2

Correlations used in literature to describe external mass transfer around cylindrical Pd-based membranes in an empty vessel.

#	Correlation	d_h	Reference
L1	$\overline{Sh}_L = 6.18$	$\frac{4A_c}{P}$	Boon et al. [21], Nordio et al. [27], Brenco et al. [28]
L2	$\overline{Sh}_L = 9.09$, for $\frac{I_{in}}{I_{out}} = 0.18$	$\frac{4A_c}{P}$	[39]
L3	$\overline{Sh}_L = 1.87 \cdot Re_L^{1.08} \cdot Sc_L^{1.08} = 1.87 \cdot Pe_L^{1.08}$	L	Catalano et al. [24]
L4	$\overline{Sh}_L = 1.87 \cdot Re_L^{0.50} \cdot Sc_L^{0.33}$	L	Catalano et al. [20]
L5	$Sh_z = 1.95 \cdot \left(Re_z \cdot Sc_z \cdot \frac{d_h}{L} \right)^{0.33} = 1.95 \cdot Gz_z^{0.33}$	$\frac{4A_c}{P}$	Caravella et al. [25]
L6	$Sh_z = 1.62 \cdot \left(Re_z \cdot Sc_z \cdot \frac{d_h}{L} \right)^{0.33} = 1.62 \cdot Gz_z^{0.33}$, for $Re \leq 2,100$	$\frac{4A_c}{P}$	Caravella et al. [19]
L7	$Sh_z = 0.332 \cdot Re_z^{0.50} \cdot Sc_z^{0.33}$, for $Sc \geq 0.6$	$\frac{4A_c}{P}$	Analytical solution for flat plate [40]
L8	$\overline{Sh}_L = 0.664 \cdot Re_L^{0.50} \cdot Sc_L^{0.33}$, for $Sc \geq 0.6$	$\frac{4A_c}{P}$	Analytical solution for flat plate [23,40]

where A_c is the cross-sectional area through which the fluid flows and P is the wetted perimeter of solid surfaces in contact with the fluid flow. When this definition is applied for the tubular membrane configuration, the following expression is obtained.

$$d_h = 4 \cdot \frac{A_{c,vessel} - A_{c,memb}}{P_{vessel} + P_{memb}} = \frac{(D_{vessel}^2 - D_{memb}^2)}{D_{vessel} + D_{memb}} = D_{vessel} - D_{memb} \quad (8)$$

The differences among the various Sherwood correlations from literature, shown in Table 2, have a huge impact on the mass transfer coefficient prediction. To demonstrate this, in Fig. 6 different mass transfer coefficients were calculated using Equation (5) containing each correlation from Table 2, with varying Reynolds number and assuming a constant Schmidt number (in gaseous mixtures, Schmidt numbers are typically always close to unity). The graph shows that the values of k_g differ consistently depending on the used correlation, even though they are all used for hydrogen permeation through tubular membranes in an empty vessel, especially for high Reynolds numbers. This indicates that each of these correlations is very case-specific and therefore should not be adopted without any further validation.

To evaluate the prediction of the mass transfer behavior, each correlation was inserted into the model and used to describe the 423 experimental datapoints obtained during the test campaign. The error between the modelled and experimental results was expressed in terms of Relative Error (RE), which was calculated for each datapoint ac-

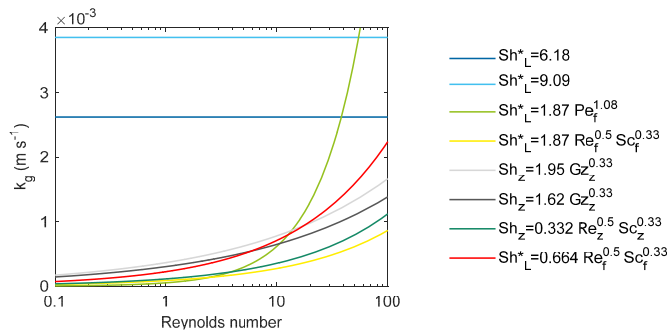


Fig. 6. Effect of Reynolds number on the mass transfer coefficient, calculated using different correlations from literature (see Table 3). Calculations were done with: $Sc = 0.5$; $L = 0.467$ m; $D_{memb} = 0.014$ m; $D_{vessel} = 0.078$ m; $D_{H_2-N_2} = 0.271$ $\mu Pa \cdot s$.

ording to the following equation.

$$RE = \frac{\bar{N}_{H_2, mod} - \bar{N}_{H_2, exp}}{\bar{N}_{H_2, exp}} \times 100\% \quad (9)$$

The obtained error distributions of the selected correlations are summarized in Fig. 7 in the form of a box plot – which is an effective approach of showing and comparing the error distribution of multiple cases in one graph [41]. The box comprises half of the datapoints with the lowest error and the line dividing the box indicates the median. The whiskers enclose the other half of the datapoints, while the outliers (2.5 IQR) are indicated with markers.

The box plots in Fig. 7 show that data fitting of each correlation listed in Table 2 gave a widespread of errors, when compared to the experimental data. One reason why these correlations perform so differently is that they are derived in different ways. Correlation L1 assumes a constant Sherwood number regardless of the conditions or geometry. The work of Boon et al. first used this number to describe the mass transfer coefficient around a tubular Pd-based membrane [21]. From this work, the number was adopted by other authors to describe the external mass transfer behavior of other tubular membranes without considering the different dimensions of their system [27,28]. The number originates from Nusselt number calculations for a concentric annular duct with insulated outer wall and an inner wall with constant heat flux [39]. The specific value of 6.18 is only relevant for a $r_{in}/r_{out} = r_{memb}/r_{vessel} = 0.5$, and therefore does not specifically fit for modules with different dimensions. The membrane module used in this work has a $r_{in}/r_{out} = 0.18$, which results in a Sherwood number of 9.09 according to correlation L2 [39]. Correlations L3-4, used by Catalano et al. were fitted

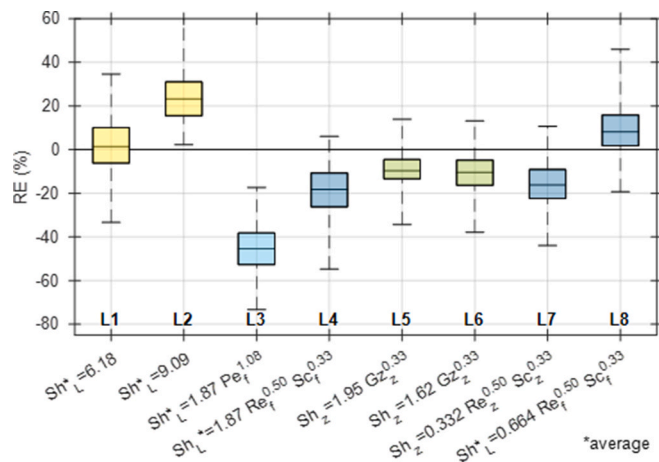


Fig. 7. Box plot of the performance of correlations used in literature.

using experimental data of a tubular Pd-based membrane [20,24]. Correlations L5-6, used by Caravella et al. originate from an analytical derivation to describe the extended Graetz problem by Sellars et al. [19, 25,42]. The extended Graetz problem is defined as heat transfer for fully-developed laminar flow in a round tube or flat conduct with either constant wall heat flux or linear wall temperature [43]. Correlations L7-8 were derived analytically to describe the boundary layer in steady laminar flow along a flat plate, and were obtained using the Blasius solution [40,44].

Another important factor that must be taken into consideration when selecting an empirical mass correlation for the mass transfer coefficient is the geometry of the system considered. The membrane separator is in fact a concentric annular duct where the parallel flow is developing both hydrodynamically and concentration-wise. Developing flow makes it hard to predict the mass transfer behavior due to the different behavior taking place in the entrance region. Furthermore, the impact of a radial velocity gradient is often neglected when modelling the hydrodynamics of a mass transfer system. However, due to the high permeance of some membranes such as the Pd-based used in this work, a significant convective contribution to mass transfer in the radial direction can be expected. To check the relative importance of a radial velocity contribution, the u_{radial}/u_{axial} ratio was also calculated for each datapoint based on the observed flux. u_{radial} is simply the volumetric permeation flux and u_{axial} was estimated by taking the gas velocity at the inlet. The ratio is on average 0.12 for the entire dataset and it varies between 0.004 and 0.450, illustrating that the velocity profile will be significantly distorted due to the high permeation flux. Finally, most suggested correlations in literature for mass transfer are based on the heat and mass transfer analogy, where most of the time a direct translation is made from heat transfer behavior to mass transfer behavior. The problem with this is that for heat transfer problems, radial convection is often neglected, whereas for mass transfer around highly permeable membrane, it might be an important factor. Summarizing the above, each correlation taken from literature has its limitations, therefore, carefully selecting a correlation or fitting a custom correlation for a specific membrane system is important.

4.4. Fitting mass transfer correlations

Since none of the mass transfer correlations was able to accurately describe the mass transfer behavior of the membranes tested in this work, a custom mass transfer correlation was fitted. The dataset obtained from the H_2/N_2 mixture tests was used to derive a Sherwood correlation that can be used to describe external mass transfer around the highly permeable Pd-Ag membrane. In Table 2, it was shown that correlations used for similar systems describe the Sherwood number as a function of the Reynolds number, the Schmidt number and the ratio of hydraulic diameter and axial dimension. Below the general forms for local and average Sherwood correlations are shown.

$$Sh_z = f\left(Re_z, Sc_z, \frac{d_h}{z}\right) \quad (10)$$

$$\bar{Sh}_L = f\left(Re_L, Sc_L, \frac{d_h}{L}\right) \quad (11)$$

Due to the complexity of modelling a system where the mass transfer coefficient is dependent on the conditions at the outlet (Re_L and Sc_L), these values will be replaced by the values in the feed (Re_f and Sc_f). The included variables contain information about the nature of the fluid and the geometry of the system. The Reynolds and Schmidt numbers are typically included since they summarize the characteristics of a mass transfer system with forced convective flow [45]. The Reynolds number is defined as the ratio of inertial and viscous forces.

$$Re = \frac{\rho u d_h}{\mu} \quad (12)$$

It is an important parameter to consider in a gas-phase mass transfer system since viscous forces slow down mass transfer in the gas phase around the membrane. On the other hand, the inertial forces diminish radial concentration profiles and therefore accelerate the mass transfer in the surroundings of the membrane.

The Schmidt number is defined as the ratio of momentum and mass diffusivities. It contains relevant information about the properties of the fluid in the operating conditions [40].

$$Sc = \frac{\mu}{\rho D_{H_2-N_2}} \quad (20)$$

In Table 3, a selection of nine different expressions (E1-9) for Sherwood correlations can be found, together with the fitting results of each correlation with the adopted model.

To assess the difference in external mass transfer behavior among the different lengths of the membrane, expression E1 was fitted for each membrane length separately and combined. The Sherwood numbers obtained from data fitting show that, for each membrane length, a different number arises. The obtained values still have a significant error, meaning that the actual behavior is not accurately captured by the expression of the correlation. Therefore, calculating the mass transfer coefficient in the gas-phase using a constant value for the Sherwood number would lead to less accurate prediction of the mass transfer coefficient. The main reason for this is that hydrodynamics and gas properties affect the mass transfer coefficient, and these effects are not accounted for when only considering a constant Sherwood number. Besides that, depletion caused by hydrogen permeation could cause local differences in flow pattern and gas composition. These two parameters are important to predict the mass transfer coefficient, and therefore, local differences in mass transfer coefficient can be expected. In Fig. 8, an example of an axial profile generated by the model is shown. Results show the significantly changing gas velocity and gas-composition along the length of the 467 mm long membrane.

The differences among the fitted values of the Sherwood numbers in Table 3 indicates that there is a certain dependence of the mass transfer coefficient on the length or axial coordinate. Possible explanations for this dependence could be either entrance effects or the changing conditions due to hydrogen depletion. Entrance effects would lead to local differences in the mass transfer coefficient, which would have a much bigger impact for smaller membranes than for larger membranes. In the entrance region, a higher mass transfer rate could be expected since concentration polarization profiles still need to settle. Additionally, the average gas velocity is higher for a shorter membrane, also leading to higher observed mass transfer coefficient. The alternative explanation is the local differences induced by hydrogen depletion. Gas velocity, hydrogen fraction and flux are all changing with the axial coordinate. Gas velocity could change the

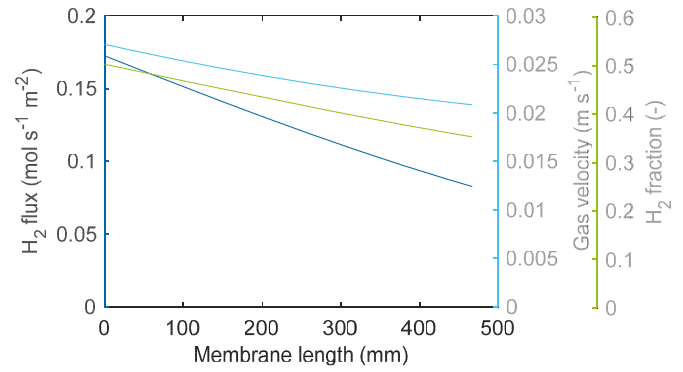


Fig. 8. Axial profile of gas velocity, hydrogen fraction and hydrogen flux generated by the model with fitted parameters of L-467. $x_{H_2}(\text{feed}) = 0.50$, $F_v(\text{feed}) = 15 \text{ ln min}^{-1}$, $p_{\text{ret}} = 5 \text{ bar(a)}$ and $T = 400 \text{ }^\circ\text{C}$. Calculations were done with $Sh_L = 10$.

hydrodynamics of the system, hydrogen fraction affects the local gas properties, and the hydrogen flux impacts the overall velocity profile. Any of these effects could cause a difference in effective mass transfer coefficient when comparing membranes of different lengths, and therefore a different overall Sherwood number is possible.

Using a constant Sherwood number for the entire membrane length did not yield a correlation that could be used to describe the mass transfer coefficient accurately. The expressions used for fitting the Sherwood correlations need more complexity, this is typically done by including exponential terms with the Reynolds and Schmidt numbers [40,46,47]. To evaluate the existence/strength of the dependencies on these dimensionless numbers, a sensitivity analysis was performed using the fitting model. The dataset was fitted to expression E3 from Table 3, while keeping the exponents of the Schmidt and Reynolds numbers fixed for different cases. In Fig. 9, the results of the sensitivity analysis are reported and show that the impact of the Re-exponent is significantly larger than the impact of the Sc-exponent. This means that hydrodynamics plays an important role in the prediction of the mass transfer coefficient.

After assessing the importance of the Re and Sc numbers when predicting the Sherwood number, expressions including these dimensionless numbers were fitted. In Table 3 and Fig. 10, the results of fitting expressions E1-4 can be compared. The accuracy increased significantly upon the addition of dependence on the Reynolds number, demonstrating that hydrodynamics is a relevant aspect to be included. Also giving an additional degree of freedom in terms of the dependency on

Table 3

Different expressions for Sherwood correlations used in literature [20,23,25,39,40,45–48], together with the fitting results.

#	General form	Fitted correlation	\overline{RE}^*	RE_{10}^{**}
E1	$\overline{Sh}_L = a_1$	$\overline{Sh}_L = 9.661 \text{ (L-150)}$	6.85%	74.47%
		$\overline{Sh}_L = 7.044 \text{ (L-300)}$	9.86%	50.35%
		$\overline{Sh}_L = 6.081 \text{ (L-467)}$	10.70%	43.97%
		$\overline{Sh}_L = 7.878 \text{ (All data)}$	9.75%	54.14%
E2	$Sh_z = a_1 \cdot Re_z^{a_2}$	$Sh_z = 1.452 \cdot Re_z^{0.44}$	6.85%	79.91%
E3	$Sh_z = a_1 \cdot Re_z^{0.5} \cdot Sc_z^{0.33}$	$Sh_z = 1.531 \cdot Re_z^{0.50} \cdot Sc_z^{0.33}$	6.27%	83.69%
E4	$Sh_z = a_1 \cdot Re_z^{a_2} \cdot Sc_z^{a_3}$	$Sh_z = 1.356 \cdot Re_z^{0.57} \cdot Sc_z^{0.47}$	6.16%	85.82%
E5	$Sh_z = a_1 \cdot Pe_z^{a_2}$	$Sh_z = 1.452 \cdot Pe_z^{0.58}$	6.15%	86.05%
E6	$\overline{Sh}_L = a_1 \cdot Re_L^{a_2} \cdot Sc_L^{a_3}$	$\overline{Sh}_L = 1.186 \cdot Re_L^{0.53} \cdot Sc_L^{0.22}$	6.95%	78.96%
E7	$\overline{Sh}_L = a_1 \cdot Pe_L^{a_2}$	$\overline{Sh}_L = 1.566 \cdot Pe_L^{0.53}$	7.21%	71.87%
E8	$Sh_z = a_1 \cdot \left(Re_z \cdot \frac{d_h}{z} \right)^{a_2} \cdot Sc_z^{a_3}$	$Sh_z = 2.015 \cdot \left(Re_z \cdot \frac{d_h}{z} \right)^{0.62} \cdot Sc_z^{0.76}$	2.65%	96.22%
E9	$Sh_z = a_1 \cdot Gz_z^{a_2}$	$Sh_z = 1.846 \cdot Gz_z^{0.60}$	2.77%	95.51%

* $\overline{RE} = \langle |RE| \rangle$, ** $RE_{10} =$ percentage within $\pm 10\%$ error.

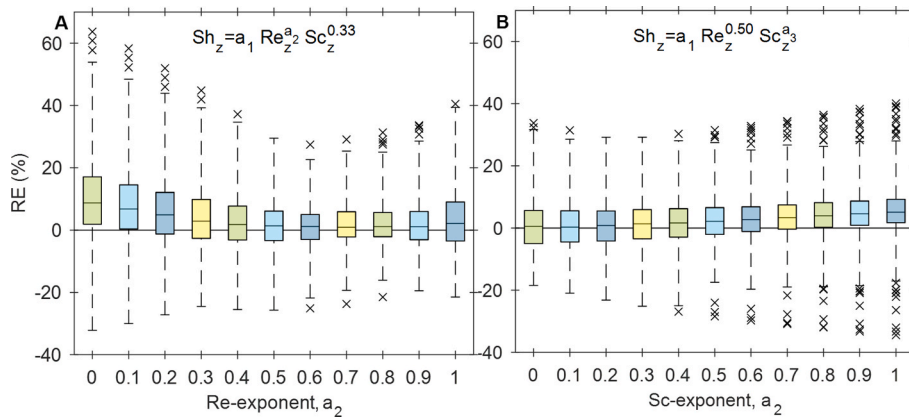


Fig. 9. Box plot of the results of the sensitivity analysis on the Re- (A) and Sc- (B) exponents.

the Schmidt number improved accuracy as well, but it was not as impactful as the Reynolds dependency. Fixing the exponents to 0.50 and 0.33 (in expression E3) still gives an accuracy close to expression E4 with freely fitted exponents. This means that the fitted values of these exponents are in line with literature data, since 0.50 and 0.33 are the values most frequently appearing in literature for cylindrical mass and heat transfer systems with forced laminar flows [40,45–47].

In literature, some works use a correlation predicting the averaged Sherwood number (Table 3: 1–4&8) and some use a locally predicted Sherwood number (Table 2: 5–7). To evaluate whether the use of local or average Sherwood numbers improves the accuracy of the model, two different expressions were fitted both for the average and local form. Comparing E4-5 to E6-7 in Table 3 and Fig. 10, allows to compare the average and local approach. In general, the local correlations seem to be more accurate than the average correlations. This is because the local correlations can account for local differences occurring over the length of the membrane. These differences arise due to depletion and developing flow.

By looking at E4 and E5, a comparison can also be made based on whether combining the Reynolds and Schmidt terms into one Peclet term is desirable. Results show that using a single Peclet term does not significantly reduce the accuracy of the correlation. This means that the expression can be simplified to a form with only two fitted parameters instead of three without lowering the accuracy.

To further improve the accuracy and/or increase the robustness of the Sherwood correlation, expressions E8-9 were also used for data

fitting. Looking at the fitting results in Table 3 and Fig. 10, it can be seen that upon the addition of the d_h/z ratio, the accuracy improved significantly compared to expression E5. When expressions E8 and E9 are compared, it can also be concluded that the exponential terms can be combined into one without a significant cost in terms of accuracy. The remaining correlation includes only the Graetz ($Gz = Sc \cdot Re \cdot d_h/z$) number exponential term and just 2 fitted parameters are required.

5. Discussion

The correlations fitting in the previous paragraph allows to draw the following points:

- An overall constant value of the Sherwood number, leading to a constant value of the mass transfer coefficient in the film layer model, is typically not accurate enough to describe the concentration polarization phenomena in a membrane separation module. Only 54.14% of the predicted values are within a relative error of 10% with the experimental results.
- Using a constant value of the Sherwood number calculated averagely (in this work, using the inlet conditions), assuming that it is constant along the membrane, but it changes depending on the inlet conditions, improves the performance: up to 78.96% of the predictions are within 10% of relative error with experimental data.
- It is possible to further improve the fitting by considering a local formulation of the Sherwood number. Up to 86.05% of the predicted

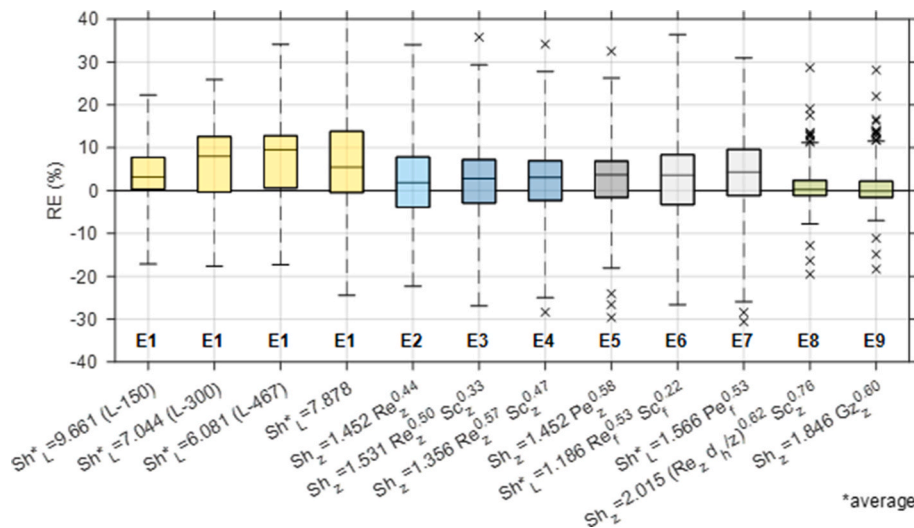


Fig. 10. Box plot of the performance of each fitted correlation shown in Table 3.

values can fall in the 10% range of the relative error using a formulation dependent on the Peclet number.

- An even better fitting can be found by introducing the dependence on the axial position z . In this case, 96.22% of the data points were reproduced within the 10% relative error. To simplify the fitting, the Graetz number can be used instead of fitting Re and Sc separately, preferring the formulation simplicity over a small loss of accuracy (95.51% of the data are then in the 10% relative error range).

Therefore, the best correlation fitted in this work is the following expression.

$$Sh_z = 1.846 \cdot \left(Re_z \cdot Sc_z \cdot \frac{d_h}{z} \right)^{0.60} = 1.846 \cdot Gz_z^{0.60} \quad (13)$$

Where the Graetz number is:

$$Gz = Re \cdot Sc \cdot \frac{d_h}{z} = \frac{\rho v d_h}{\mu} \cdot \frac{\mu}{\rho D} \cdot \frac{d_h}{z} = \frac{v d_h^2}{D_{H_2-N_2} z} \quad (14)$$

It typically describes laminar flow in a channel. For the experiments Reynolds numbers varied from 6 to 150 ($\overline{Re} = 37$), meaning that the flow was laminar. The Graetz numbers calculated half-way the membrane varied from 2 to 25 ($\overline{Gz} = 8$), these values are sufficiently low to assume that flow is fully developed. Binary hydrogen-nitrogen diffusivity is always a near-constant parameter in the conditions of the experiments, same as the hydraulic diameter. Thus, the two parameters actively affecting the Sherwood number and thus the mass transfer coefficient are the fluid velocity and the axial coordinate z .

Regarding fluid velocity, it was observed that the experimental results in Fig. 5 for the three different membrane lengths were almost identical at the same F/A ratio. This means that, in case of a double membrane length (or membrane area), the inlet flow rate and therefore also the gas velocity are doubled. This suggests that the gas velocity through the vessel does not affect, in the range investigated, the external mass transfer, and thus permeation performance, in a significant way.

Additionally, the matching mass transfer behavior at the same F/A ratio suggests that there is not an important effect of the membrane length by itself, ruling out a strong impact of entrance effects. However, data-fitting indicated that the inclusion of the axial coordinate is significantly beneficial for the performance of the correlation.

Furthermore, it was also observed that the overall mass transfer behavior is significantly impacted with changes in the hydrogen content. Both Richardson's equation and the film layer model itself include dependencies on the hydrogen fraction but the experimental results suggest an additional dependency on the hydrogen content. The presence of the axial coordinate at the denominator, increasing over the membrane length, and of velocity at the numerator, decreasing with membrane length, very likely support the film layer model to describe the flux reduction due to a decrease in hydrogen content.

A function describing the mass transfer coefficient including the dependence of the hydrogen content seems in general complex and case dependent, and it is difficult to match this relation with the simplicity required by a model. The fitted correlation in this work provides a powerful tool to reproduce several datapoints with a relatively simple expression.

6. Conclusions

In this work, one Pd-based membrane was tested at three different lengths. First, permeation tests were performed in pure hydrogen and nitrogen to determine the Richardson's parameters and ideal permselectivity. Then H_2/N_2 mixture tests were performed to analyze the external mass transfer impact on hydrogen permeation and to generate a dataset that can be used for external mass transfer modelling.

The results of the H_2/N_2 mixture tests indicate that in membrane systems with highly permeable Pd-based membranes in an empty vessel,

the permeation behavior is dominated by the effects of concentration polarization and hydrogen depletion.

The observations from the mixture experiments were taken into consideration during construction of the model. Depletion was accounted for by discretizing the membrane area in the axial direction and concentration polarization was covered by the inclusion of a film layer model with empirical Sherwood correlation.

To determine the best Sherwood correlation to predict the external mass transfer behavior of the membrane system used in this work, eight different correlations taken from literature and used in similar systems were discussed and evaluated. However, none of these correlations were able to accurately predict the mass transfer behavior observed during the mixture tests. Therefore, a new correlation was constructed and fitted. Different expressions including different parameters were considered and the best expression was selected. Significant improvement compared to the correlations available in literature was achieved: while best results from literature correlation came from a constant Sherwood value and was able to represent 55.32% of the experimental results in the 10% relative error range, the correlation fitted for this work on several experimental conditions was able to reproduce in that range 95.51% of them.

Fig. 11 shows a comparison of the four different correlations tested or fitted in this work. The best performing literature correlation (L1), the most frequently appearing expression ($Sh = a_1 \cdot Re^{a_2} \cdot Sc^{a_3}$), as averaged (E6) and local (E4) correlation and the best fitted correlation in this work (E9). The fitted correlation using expression E9 shows a much higher accuracy than the other three correlations, indicating that the accuracy of the prediction of the mass transfer coefficient can be significantly enhanced when using the right empirical correlation.

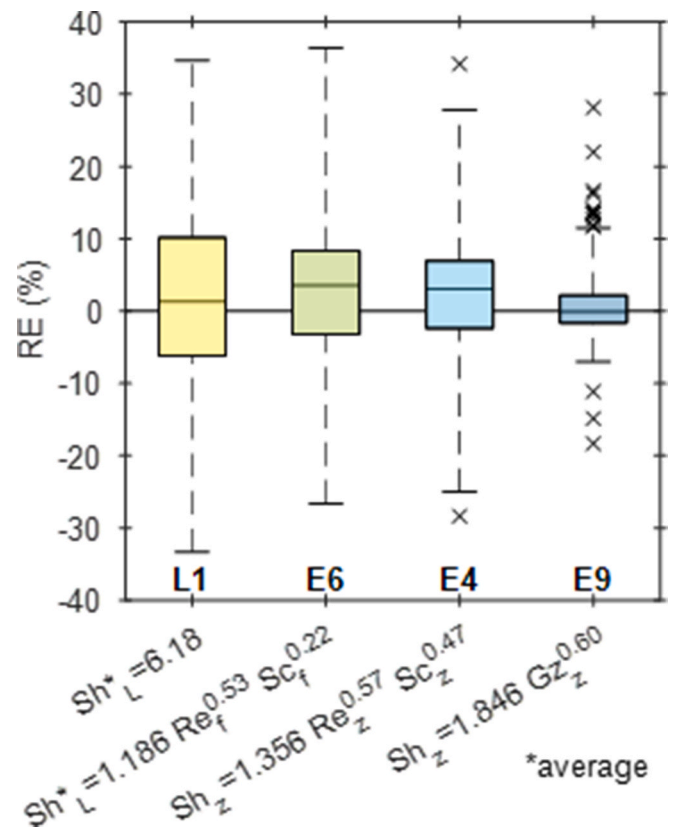


Fig. 11. Box plot of the performance of a selection of correlations used in this work.

CRedit authorship contribution statement

W.J.R. Ververs: Conceptualization, Formal analysis, Investigation, Writing – original draft. **M. Ongis:** Investigation, Methodology. **A. Arratibel:** Investigation, Writing – review & editing. **L. Di Felice:** Supervision, Writing – review & editing. **F. Gallucci:** Conceptualization, Funding acquisition, Supervision, Writing – review & editing.

Acknowledgments

This work has received funding from the European Union’s Horizon 2020 Research and Innovation Program under grant agreement No 869896 (MACBETH).

Appendix A. Supplementary data

Supplementary data to this article can be found online at <https://doi.org/10.1016/j.ijhydene.2024.04.337>.

Nomenclature*Letters*

a	Empirical factor
A	Membrane area, m ²
A _c	Cross sectional area of retentate, m ²
c _{tot}	Total molar concentration, mol m ⁻³
d _h	Hydraulic diameter, m
D	Diffusion coefficient, m ² s ⁻¹
D	Diameter, m
E _a	Activation energy, J mol ⁻¹
F	Molar flow, mol s ⁻¹
F _v	Volumetric flow, ln min ⁻¹
Gz	Graetz number
ID	Inner diameter, mm
IQR	Inter quartile range
k _g	Mass transfer coefficient, m s ⁻¹
L	Length, m
n	Pressure exponent
N	Molar flux, mol s ⁻¹ m ⁻²
OD	Outer diameter, mm
p	Partial pressure, Pa
P	Perimeter, m
Pe	Permeance, mol s ⁻¹ m ⁻² bar ⁻¹
Pe	Peclet number
Pe ₀	Pre-exponential factor of permeance, mol s ⁻¹ m ⁻² Pa ⁻ⁿ
r	Radius, m
R	Universal gas coefficient, J mol ⁻¹ K ⁻¹
Re	Reynolds number
RE	Relative Error, %
RF	Recovery factor, %
S	Selectivity
Sc	Schmidt number
Sh	Sherwood number
T	Temperature, K
u	Gas velocity, m s ⁻¹
x	Molar fraction
y	Radial coordinate, m
z	Axial coordinate, m

Greek letters

δ	Film layer thickness, m
μ	Dynamic viscosity, Pa s
ρ	Mass density, kg m ⁻³

Subscripts

exp	Experimental
f	Feed
in	Inner
L	At position z = L
memb	Membrane

mod	Model
out	Outer
perm	Permeate
ret	Retentate
z	At position z

References

- [1] Midgley G, Hannah L. Extinction risk from climate change. *Biodivers Clim Chang Transform Biosph* 2019;294–6. <https://doi.org/10.2307/j.ctv8jnz1.37>.
- [2] Hosseini SE, Wahid MA. Hydrogen production from renewable and sustainable energy resources: promising green energy carrier for clean development. *Renew Sustain Energy Rev* 2016;57:850–66. <https://doi.org/10.1016/j.rser.2015.12.112>.
- [3] Sholl DS, Lively RP. Seven chemical separations. *Nature* 2016;532:435–7.
- [4] Gallucci F, Fernandez E, Corengia P, van Sint Annaland M. Recent advances on membranes and membrane reactors for hydrogen production. *Chem Eng Sci* 2013; 92:40–66. <https://doi.org/10.1016/j.ces.2013.01.008>.
- [5] Nordio M, Melendez J, van Sint Annaland M, Pacheco Tanaka DA, Llosa Tanco M, Gallucci F. Comparison between carbon molecular sieve and Pd-Ag membranes in H₂-CH₄ separation at high pressure. *Int J Hydrogen Energy* 2020;45(53): 28876–92. <https://doi.org/10.1016/j.ijhydene.2020.07.191>.
- [6] Nordio M, Wassie SA, Van Sint Annaland M, Pacheco Tanaka DA, Viviente Sole JL, Gallucci F. Techno-economic evaluation on a hybrid technology for low hydrogen concentration separation and purification from natural gas grid. *Int J Hydrogen Energy* 2021;46(45):23417–35. <https://doi.org/10.1016/j.ijhydene.2020.05.009>.
- [7] Gallucci F, Basile A. Pd-Ag membrane reactor for steam reforming reactions: a comparison between different fuels. *Int J Hydrogen Energy* 2008;33(6):1671–87. <https://doi.org/10.1016/j.ijhydene.2008.01.010>.
- [8] Dittmeyer R, et al. Micro and micro membrane reactors for advanced applications in chemical energy conversion. *Curr Opin Chem Eng* 2017;17(September):108–25. <https://doi.org/10.1016/j.coche.2017.08.001>.
- [9] Mosca L, et al. Process design for green hydrogen production. *Int J Hydrogen Energy* 2020;45(12):7266–77. <https://doi.org/10.1016/j.ijhydene.2019.08.206>.
- [10] Spallina V, et al. Direct route from ethanol to pure hydrogen through autothermal reforming in a membrane reactor: experimental demonstration, reactor modelling and design. *Energy* 2018;143:666–81. <https://doi.org/10.1016/j.energy.2017.11.031>.
- [11] Ribeirinha P, Abdollahzadeh M, Boaventura M, Mendes A. H₂ production with low carbon content via MSR in packed bed membrane reactors for high-temperature polymeric electrolyte membrane fuel cell. *Appl Energy* 2017;188:409–19. <https://doi.org/10.1016/j.apenergy.2016.12.015>.
- [12] Gallucci F, Basile A, Tosti S, Iulianelli A, Drioli E. Methanol and ethanol steam reforming in membrane reactors: an experimental study. *Int J Hydrogen Energy* 2007;32(9):1201–10. <https://doi.org/10.1016/j.ijhydene.2006.11.019>.
- [13] Cechetto V, Di Felice L, Medrano JA, Makhlofi C, Zuniga J, Gallucci F. H₂ production via ammonia decomposition in a catalytic membrane reactor. *Fuel Process Technol* 2021;216(January):106772. <https://doi.org/10.1016/j.fuproc.2021.106772>.
- [14] Cechetto V, Di Felice L, Gutierrez Martinez R, Arratibel Plazaola A, Gallucci F. Ultra-pure hydrogen production via ammonia decomposition in a catalytic membrane reactor. *Int J Hydrogen Energy* 2022;47(49):21220–30. <https://doi.org/10.1016/j.ijhydene.2022.04.240>.
- [15] Cerrillo JL, et al. High purity, self-sustained, pressurized hydrogen production from ammonia in a catalytic membrane reactor. *Chem Eng J* 2022;431(December 2021). <https://doi.org/10.1016/j.cej.2021.134310>.
- [16] Anonymous. H₂SITE inaugurates the first production plant for palladium alloy membranes to obtain hydrogen. *Businesswire* 2022 [Online]. Available: <https://www.businesswire.com/news/home/20221115005287/en/H2SITE-inaugurates-the-first-production-plant-for-palladium-alloy-membranes-to-obtain-hydrogen>. [Accessed 27 March 2023].
- [17] Arratibel A, Pacheco Tanaka A, Laso I, van Sint Annaland M, Gallucci F. Development of Pd-based double-skinned membranes for hydrogen production in fluidized bed membrane reactors. *J Membr Sci* 2018;550(August 2017):536–44. <https://doi.org/10.1016/j.memsci.2017.10.064>.
- [18] Gallucci F, Van Sintannaland M, Kuipers JAM. Theoretical comparison of packed bed and fluidized bed membrane reactors for methane reforming. *Int J Hydrogen Energy* 2010;35(13):7142–50. <https://doi.org/10.1016/j.ijhydene.2010.02.050>.
- [19] Caravella A, Barbieri G, Drioli E. Concentration polarization analysis in self-supported Pd-based membranes. *Sep Purif Technol* 2009;66(3):613–24. <https://doi.org/10.1016/j.seppur.2009.01.008>.
- [20] Catalano J, Giacinti Baschetti M, Sarti GC. Influence of the gas phase resistance on hydrogen flux through thin palladium-silver membranes. *J Membr Sci* 2009;339(1–2):57–67. <https://doi.org/10.1016/j.memsci.2009.04.032>.
- [21] Boon J, Li H, Dijkstra JW, Pieterse JAZ. 2-Dimensional membrane separator modelling: mass transfer by convection and diffusion. *Energy Proc* 2011;4: 699–706. <https://doi.org/10.1016/j.egypro.2011.01.108>.
- [22] Peters TA, Stange M, Klette H, Bredesen R. High pressure performance of thin Pd-23%Ag/stainless steel composite membranes in water gas shift gas mixtures; influence of dilution, mass transfer and surface effects on the hydrogen flux. *J Membr Sci* 2008;316(1–2):119–27. <https://doi.org/10.1016/j.memsci.2007.08.056>.
- [23] Hou K, Hughes R. The effect of external mass transfer, competitive adsorption and coking on hydrogen permeation through thin Pd/Ag membranes. *J Membr Sci* 2002;206(1–2):119–30. [https://doi.org/10.1016/S0376-7388\(01\)00770-0](https://doi.org/10.1016/S0376-7388(01)00770-0).
- [24] Catalano J, Giacinti Baschetti M, Sarti GC. Influence of water vapor on hydrogen permeation through 2.5 μm Pd-Ag membranes. *Int J Hydrogen Energy* 2011;36(14):8658–73. <https://doi.org/10.1016/j.ijhydene.2011.03.139>.
- [25] Caravella A, Hara S, Drioli E, Barbieri G. Sieverts law pressure exponent for hydrogen permeation through Pd-based membranes: coupled influence of non-ideal diffusion and multicomponent external mass transfer. *Int J Hydrogen Energy* 2013;38(36):16229–44. <https://doi.org/10.1016/j.ijhydene.2013.09.102>.
- [26] Boon J, Pieterse JAZ, Dijkstra JW, van Sint Annaland M. Modelling and systematic experimental investigation of mass transfer in supported palladium-based membrane separators. *Int J Greenh Gas Control* 2012;11(SUPPL):122–9. <https://doi.org/10.1016/j.ijggc.2012.09.014>.
- [27] Nordio M, et al. Effect of sweep gas on hydrogen permeation of supported Pd membranes: experimental and modeling. *Int J Hydrogen Energy* 2019;44(8): 4228–39. <https://doi.org/10.1016/j.ijhydene.2018.12.137>.
- [28] Brencio C, Fontein FWA, Medrano JA, Di Felice L, Arratibel A, Gallucci F. Pd-based membranes performance under hydrocarbon exposure for propane dehydrogenation processes: experimental and modeling. *Int J Hydrogen Energy* 2022;47(21):11369–84. <https://doi.org/10.1016/j.ijhydene.2021.09.252>.
- [29] Ververs WJR, Arratibel Plazaola A, Di Felice L, Gallucci F. Dataset - H₂/N₂ mixture experiments with PdAg membrane. *Zenodo* 2023. <https://doi.org/10.5281/zenodo.7961792>.
- [30] Gallucci F, Richardson law. In: Drioli E, Giorno L, editors. *Encyclopedia of membranes*. Berlin, Heidelberg: Springer Berlin Heidelberg; 2012. p. 1–2.
- [31] Flanagan TB, Wang D. Exponents for the pressure dependence of hydrogen permeation through Pd and Pd-Ag alloy membranes. *J Phys Chem C* 2010;114(34): 14482–8. <https://doi.org/10.1021/jp101364j>.
- [32] de Nooijer N, et al. On concentration polarisation in a fluidized bed membrane reactor for biogas steam reforming: modelling and experimental validation. *Chem Eng J* 2018;348(March):232–43. <https://doi.org/10.1016/j.cej.2018.04.205>.
- [33] Song L. Why is the film model fundamentally wrong but still able to correlate the experimental data in membrane processes? *J Membr Sci* 2023;686(July):121987. <https://doi.org/10.1016/j.memsci.2023.121987>.
- [34] Zydny AL. Stagnant film model for concentration polarization in membrane systems. *J Membr Sci* 1997;130(1–2):275–81. [https://doi.org/10.1016/S0376-7388\(97\)00006-9](https://doi.org/10.1016/S0376-7388(97)00006-9).
- [35] Rohlfis W, Thiel GP, Lienhard JH. Modeling reverse osmosis element design using superposition and an analogy to convective heat transfer. *J Membr Sci* 2016;512: 38–49. <https://doi.org/10.1016/j.memsci.2016.03.049>.
- [36] Melendez J, Fernandez E, Gallucci F, van Sint Annaland M, Arias PL, Pacheco Tanaka DA. Preparation and characterization of ceramic supported ultra-thin (~1 μm) Pd-Ag membranes. *J Membr Sci* 2017;528(October 2016):12–23. <https://doi.org/10.1016/j.memsci.2017.01.011>.
- [37] Zeng G, Shi L, Liu Y, Zhang Y, Sun Y. A simple approach to uniform PdAg alloy membranes: comparative study of conventional and silver concentration-controlled co-plating. *Int J Hydrogen Energy* 2014;39(9):4427–36. <https://doi.org/10.1016/j.ijhydene.2014.01.022>.
- [38] Dittmeyer R, Höllein V, Daub K. Membrane reactors for hydrogenation and dehydrogenation processes based on supported palladium. *J Mol Catal Chem* 2001; 173(1–2):135–84. [https://doi.org/10.1016/S1381-1169\(01\)00149-2](https://doi.org/10.1016/S1381-1169(01)00149-2).
- [39] Rohsenow WM, James P H, Young C. *Handbook of heat transfer*. third ed. McGraw Hill; 1998.
- [40] Incropera FP, Dewitt DP, Bergman TL, Lavine AS. *Fundamentals of heat and mass transfer*. sixth ed. John Wiley & Sons, Inc.; 2007.
- [41] Williamson DF, Parker RA, Kendrick JS. The box plot: a simple visual method to interpret data. *Ann Intern Med* 1989;110(11):916–21.
- [42] John Sellars JK, Tribus Myron. *Heat transfer to laminar flow in a round tube of flat conduit*. 1954. p. 1–32.
- [43] Mi L, Hwang ST. Correlation of concentration polarization and hydrodynamic parameters in hollow fiber modules. *J Membr Sci* 1999;159(1–2):143–65. [https://doi.org/10.1016/S0376-7388\(99\)00046-0](https://doi.org/10.1016/S0376-7388(99)00046-0).
- [44] Blasius H. *The boundary layers in fluids with little friction* (NASA translation 1950). 1908.
- [45] Welty JR, Wicks CE, Wilson RE, Rorrer GL. *Fundamentals of momentum, heat, and mass transfer*. fifth ed. John Wiley & Sons, Inc.; 2008.

- [46] Çengel YA, Ghajar AJ. Heat and mass transfer - fundamentals & applications. fifth ed. Mc Graw Hill Education; 2015.
- [47] Baehr HD, Stephan K. Heat and mass transfer. Springer; 1998.
- [48] Ho CK, Webb SW. Gas transport in porous media. Springer; 2006.
- [50] Reid RC, Praunitz JM, Poling BE. The properties of gases and liquids. fourth ed. New York: McGraw-Hill; 1987.
- [51] Bird RB, Stewart WE, Lightfoot EE. Transport phenomena. second ed. John Wiley & Sons, Inc.; 2002.

Further reading

- [49] Poling BE, Prausnitz JM, O'Connell JP. Properties of gases and liquids. 2013.